Meteoritics & Planetary Science 38, Nr 11, 1679–1696 (2003)
Abstract available online at http://meteoritics.org

Ordinary chondrite metallography: Part 2. Formation of zoned and unzoned metal particles in relatively unshocked H, L, and LL chondrites

R. J. REISENER and J. I. GOLDSTEIN*

Department of Mechanical and Industrial Engineering and Department of Geosciences
University of Massachusetts, Amherst, Massachusetts 01003, USA
*Corresponding author. E-mail: jig0@ecs.umass.edu

(Received 16 January 2003; revision accepted 1 December 2003)

Abstract–We studied the metallography of Fe-Ni metal particles in 17 relatively unshocked ordinary chondrites and interpreted their microstructures using the results of P-free, Fe-Ni alloy cooling experiments (described in Reisener and Goldstein 2003). Two types of Fe-Ni metal particles were observed in the chondrites: zoned taenite + kamacite particles and zoneless plessite particles, which lack systematic Ni zoning and consist of tetrataenite in a kamacite matrix. Both types of metal particles formed during metamorphism in a parent body from homogeneous, P-poor taenite grains. The phase transformations during cooling from peak metamorphic temperatures were controlled by the presence or absence of grain boundaries in the taenite particles. Polycrystalline taenite particles transformed to zoned taenite + kamacite particles by kamacite nucleation at taenite/taenite grain boundaries during cooling. Monocrystalline taenite particles transformed to zoneless plessite particles by martensite formation and subsequent martensite decomposition to tetrataenite and kamacite during the same cooling process. The varying proportions of zoned taenite + kamacite particles and zoneless plessite particles in types 4–6 ordinary chondrites can be attributed to the conversion of polycrystalline taenite to monocrystalline taenite during metamorphism. Type 4 chondrites have no zoneless plessite particles because metamorphism was not intense enough to form monocrystalline taenite particles. Type 6 chondrites have larger and more abundant zoneless plessite particles than type 5 chondrites because intense metamorphism in type 6 chondrites generated more monocrystalline taenite particles. The distribution of zoneless plessite particles in ordinary chondrites is entirely consistent with our understanding of Fe-Ni alloy phase transformations during cooling. The distribution cannot be explained by hot accretion-autometamorphism, post-metamorphic brecciation, or shock processing.

INTRODUCTION

Ordinary chondrites contain 5–20 wt% Fe-Ni metal, which occurs as 1 μm to 1 mm-sized particles that are peppered throughout a matrix of olivine and pyroxene. Fe-Ni metal minerals, primarily taenite (γ) and kamacite (α), are sensitive indicators of thermal processing because the metal undergoes a variety of solid-state phase transformations including nucleation and growth, martensite formation, ordering, spinodal decomposition, and discontinuous precipitation (Yang et al. 1997; Grokhovsky and Bevan 1983). Metallographic studies of metal in ordinary chondrites have provided information about chondrite accretion temperatures (Bevan 1983; Hutchison and Bevan 1983), peak metamorphic temperatures (McCoy et al. 1991; Reisener and Goldstein 1999a), parent body cooling rates (Wood 1967; Willis and Goldstein 1981), shock processing (Bennett and McSween 1996), and brecciation (Scott and Rajan 1981; Rubin 1990).

Ordinary chondrites experienced chemical and thermal processing in nebular settings (condensation and chondrule formation) and in parent body settings (thermal metamorphism and shock metamorphism). According to the conventional model, ordinary chondrites experienced a 3-stage thermal history involving: 1) cold accretion; 2) metamorphic heating in a parent body; and 3) cooling in a parent body. This model postulates that type 3, 4, 5, and 6 ordinary chondrites experienced increasing degrees of

textural and mineralogical equilibration because they reached progressively higher metamorphic temperatures. Peak metamorphic temperatures of ordinary chondrites have been estimated using orthopyroxene-clinopyroxene thermometry and other petrographic constraints (McSween et al. 1988). The approximate peak metamorphic temperatures reached by type 3–6 ordinary chondrites are plotted on the Fe-Ni phase diagram in Fig. 1. The average metal compositions of the H, L, and LL chemical groups, calculated from wet chemical data (Jarosewich 1990), are also indicated in Fig. 1. The highly equilibrated type 4–6 ordinary chondrites reached peak metamorphic temperatures within the single-phase taenite field, and the metallographic characteristics that formed in nebular settings were erased. The metallography of type 4–6 ordinary chondrites should be relatively straightforward because the dominant microstructures and phase compositions formed during slow cooling from peak metamorphic temperatures.

Most type 4–6 ordinary chondrites contain metal particles composed of zoned taenite and kamacite (Figs. 2a and 2b).

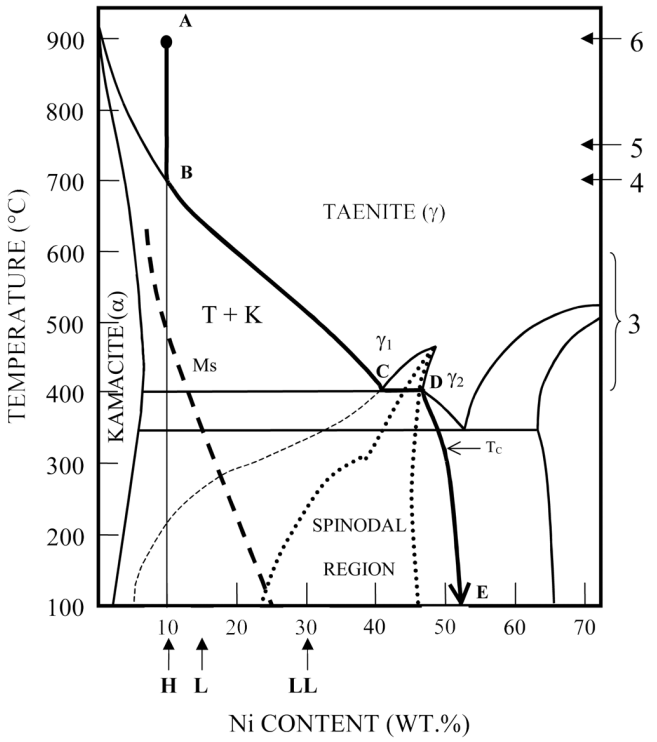

Fig. 1. Fe-Ni phase diagram showing the taenite field, kamacite field, taenite + kamacite field (T + K), and region of spinodal decomposition. Line A → E indicates the composition of taenite at the kamacite/taenite interface during cooling for an alloy of 10 wt% Ni. M_s is the martensite start line, γ_1 is paramagnetic taenite, and γ_2 is ferromagnetic taenite. T_C is the Fe-50Ni critical ordering temperature at which taenite transforms to the ordered phase, tetrataenite. The average metal Ni concentrations in H, L, and LL group ordinary chondrites are indicated. The peak metamorphic temperatures reached by type 3–6 ordinary chondrites (McSween et al. 1988) are indicated on the right hand side of the phase diagram.

The zoned taenite and kamacite phases are interpreted to have formed by the diffusion controlled transformation taenite → taenite + kamacite during cooling from peak metamorphic temperatures (see Fig. 1). The taenite and kamacite Ni zoning, including the classic "M"-shaped taenite Ni profile, is a result of incomplete transformation (Wood 1967).

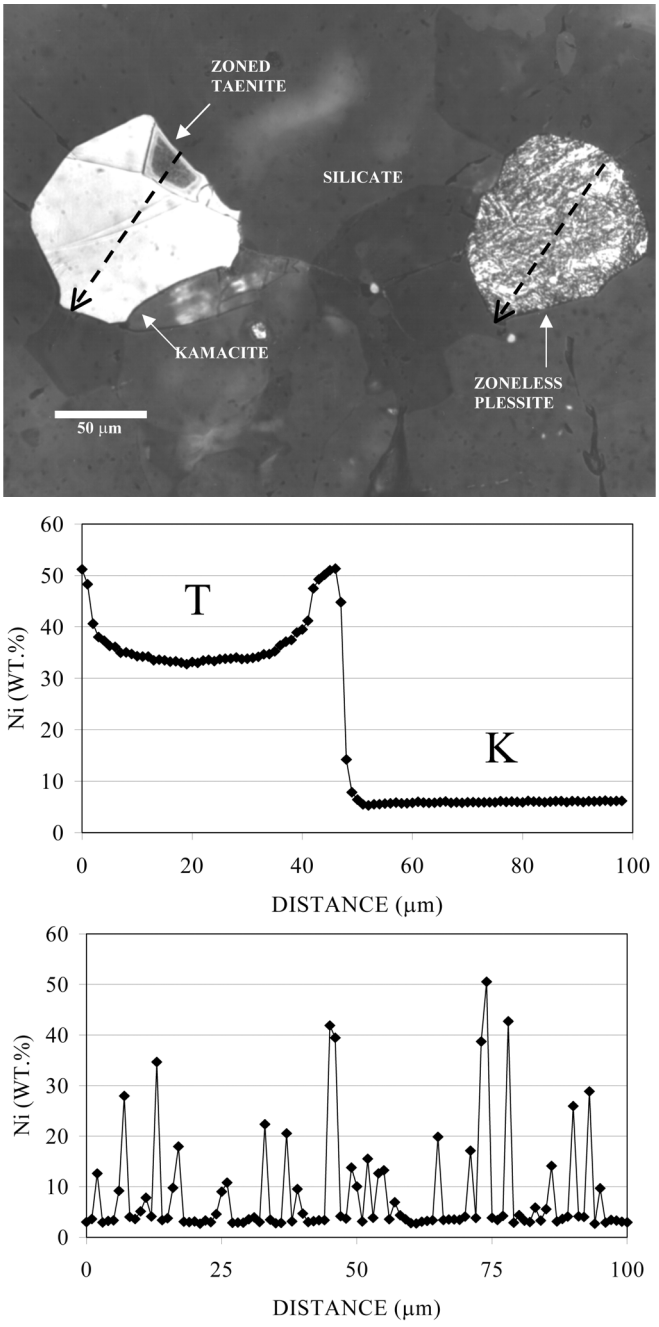

Fig. 2. a) Optical micrograph of Guarena (H6) showing a zoned taenite + kamacite particle (left) and a zoneless plessite particle (right). The broken lines on micrographs indicate the positions of microprobe traverses; b) electron microprobe Ni traverse across the zoned taenite + kamacite particle; c) electron microprobe Ni traverse across the zoneless plessite particle.

Many H5–6 and L5–6 chondrites also contain metal particles that have plessitic microstructures and lack systematic rim-to-rim Ni zoning (Figs. 2a and 2c). Sears and Axon (1975) named these metal particles "zoneless plessite particles." Zoneless plessite particles occur in close proximity to but are always isolated from zoned taenite + kamacite particles (Willis and Goldstein 1983). According to these observations, the formation of zoneless plessite particles appears to be consistent with the slow cooling of chondritic metal particles. Clearly, however, the formation of zoneless plessite particles cannot be explained in terms of the traditional taenite → taenite + kamacite reaction. Bevan (1983) and Hutchison and Bevan (1983) proposed that the presence of zoneless plessite particles in ordinary chondrites is incompatible with cold accretion and metamorphism, but compatible with a scenario involving hot accretion followed by "autometamorphism." Rubin (1990), on the other hand, suggested that zoneless plessite particles evolved independently from the host chondrite and were incorporated into chondrites during post-metamorphic brecciation.

The objectives of this paper are threefold: 1) to describe the metallography of Fe-Ni metal particles in relatively unshocked type 4–6 ordinary chondrites; 2) to develop a model for the formation of zoneless plessite particles in situ during slow cooling from peak metamorphic temperatures; and 3) to understand the process of metal microstructure development in low shock type 4–6 ordinary chondrites. To reach these objectives, we depend to a large extent on the results and conclusions of Fe-Ni alloy cooling experiments reported in a companion paper (Reisener and Goldstein 2003). The cooling experiments use P-free alloys that are compositionally similar to ordinary chondrite metal (phosphorus concentrations <0.002 wt%; Reed 1964) to determine the kamacite formation process during cooling.

EXPERIMENTAL PROCEDURE

Seventeen equilibrated (type 4–6) ordinary chondrites from the H, L, and LL chemical groups were selected for detailed metallographic studies (Table 1). Ordinary chondrites in our sample set share the following characteristics: they have low shock stages (S1–S3), they are falls or fresh finds, and they lack obvious brecciation textures. The relatively low shock stages of the samples suggest that the main metallographic structures, which formed during slow cooling, were not significantly disturbed by transient shock processing (Bennett and McSween 1996). Some of these "low shock" samples may have experienced relatively intense shock processing before cooling, but the shock features were effectively erased during subsequent annealing. The absence of brecciation textures suggests that every metal particle in a given ordinary chondrite experienced the same thermal history during cooling. Metallographic cooling rates have been measured for more than half of the samples listed in Table 1; for a given chondrite, the cooling rates of various taenite grains plot coherently, providing additional evidence that the metal particles cooled in situ. With the exception of Estacado (H6), all of the samples are observed falls, ensuring that terrestrial weathering has not significantly altered the metal. All available ordinary chondrites meeting the criteria described above were included in the study. No samples were rejected from our study due to anomalous metallographic characteristics.

The samples were polished with diamond paste from 15 μm down to 0.06 μm using standard metallographic

Table 1. Ordinary chondrites analyzed in this study.

Chondrite[a]	Class	Shock level; Reference	Cooling rate (C/Ma); Reference	Zoneless plessite?
Conquista	H4	2; Stöffler[b]	25; Taylor et al. 1987	–[c]
Forest Vale	H4	2; Rubin 1994	–	–[c]
Allegan	H5	1; Rubin 1994	15; Taylor et al. 1987	Yes
Forest City	H5	2; Stöffler et al. 1991	10; Willis and Goldstein 1981	Yes
Nuevo Mercurio	H5	1; Stöffler[b]	15; Taylor et al. 1987	Yes
Richardton	H5	1; Stöffler[b]	20; Taylor et al. 1987	Yes
Estacado	H6	1; Stöffler[b]	10; Taylor et al. 1987	Yes
Guarena	H6	1; Stöffler[b]	10; Willis and Goldstein 1981	Yes
Kernouve	H6	1; Stöffler[b]	10; Taylor et al. 1987	Yes
Portales Valley	H6	1; Kring et al. 1999	–	Yes
Bjurbole	L4	1; Stöffler[b]	2; Taylor et al. 1987	–[c]
Saratov	L4	2; Rubin 1994	–	–[c]
Elenovka	L5	2; Stöffler[b]	10; Willis and Goldstein 1981	Yes
Barwell	L5	3; Rubin 1994	–	Yes
Innisfree	LL5	2; Rubin 1994	–	No
Appley Bridge	LL6	3; Rubin 1994	–	No
St. Severin	LL6	2; Stöffler[b]	1; Willis and Goldstein 1981	No

[a]All of the ordinary chondrites, except Estacado, are observed falls.
[b]Refers to unpublished work by D. Stöffler (personal communication with E. R. D. Scott [1996]).
[c]Metal particles are too small (<5 μm) to confirm the presence of zoneless plessite.

techniques, and the metal particles were etched with Nital (2 vol% HNO_3, balance ethyl alcohol) for 20–60 sec to reveal the fine-scale microstructures. Reflected light optical microscopy was used to study the petrographic settings and microstructures of metal particles. For several ordinary chondrites, the relative proportions of opaque phases were determined by point counting through an optical microscope; approximately 500 opaque areas in each sample were randomly selected using transmitted light microscopy and subsequently identified using reflected light microscopy. A JEOL 5410 scanning electron microscope (SEM) was used for routine microstructural characterization, and a JEOL 6320 field emission scanning electron microscope was used for high resolution microstructural characterization.

The metal particles were analyzed for Fe, Ni, Co, and P using a Cameca SX50 electron microprobe operated at an accelerating voltage of 15 or 20 kV and a beam current of 15–20 nA. Counting times of 30 sec were used for each element. Fe, Ni, and Co were calibrated using pure elements; P was calibrated using schreibersite from the Grant iron meteorite. Chemical zoning profiles in the metallic phases were studied using point scans with 1 μm spacings. The bulk compositions of individual zoneless plessite particles were measured by defocusing the electron beam to a diameter of 15–20 μm (the electron beam was defocused before element calibration). X-ray intensities were reduced to wt% concentrations using the PAP φ(ρz) calculation process. The vast majority of analyses had element totals between 99 and 101 wt%.

RESULTS

Metallography of Zoned Taenite + Kamacite Particles

All of the ordinary chondrites examined in this study contain 10 μm- to 1 mm-sized metal particles composed of zoned taenite and kamacite. Zoned taenite and kamacite commonly abut troilite and chromite, and rounded blebs of silicate, troilite, and chromite occasionally occur as inclusions within the metal. Zoned taenite and kamacite sometimes appear contiguous with each other (Figs. 2–4). More commonly, zoned taenite and kamacite appear to be isolated from each other (Figs. 5 and 6). Sequential polishing, however, reveals that zoned taenite and kamacite are directly connected in 3 dimensions, as first observed by Willis and Goldstein (1983). That is, zoned taenite and kamacite always occur as zoned taenite + kamacite particles. The kamacite in ordinary chondrites does not form well-developed Widmanstätten plates such as those in iron meteorites. The shapes of taenite/kamacite interfaces vary from highly irregular (Fig. 3) to approximately planar. Taenite and kamacite occasionally exhibit a Widmanstätten-type morphology (Fig. 4), but such textures are very rare. Of the ordinary chondrites analyzed in this study, only Portales Valley (H6) contains widespread Widmanstätten-type structures. In Portales Valley, metal veins

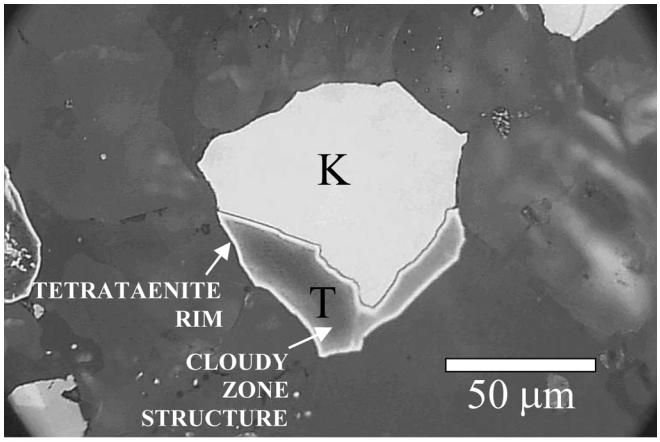

Fig. 3. Typical zoned taenite + kamacite particle in Guarena (H6). Note the irregular shape of the taenite/kamacite interface.

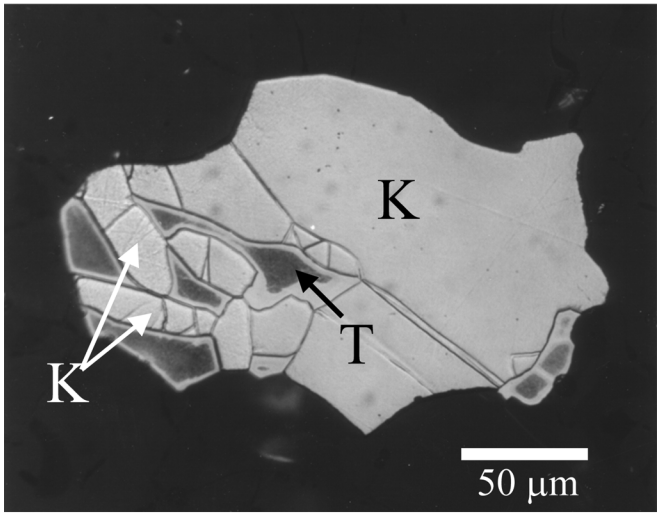

Fig. 4. Taenite + kamacite particle in Guarena (H6), which displays a Widmanstätten-like texture. The arrows indicate 2 kamacite (K) plates. The dark-etching regions between the kamacite plates are zoned taenite (T).

exhibit a well-defined Widmanstätten structure, while smaller metal particles in the silicate portion do not exhibit Widmanstätten structure or have poorly developed Widmanstätten structures similar to that shown in Fig. 4.

Zoned taenite always exhibits continuous and clear-etching tetrataenite rims (Yang et al. 1997) that are 1–3 μm thick (Figs. 2–6). Tetrataenite rims occur at taenite/kamacite, taenite/silicate, and taenite/troilite interfaces and are present whether taenite is visibly contiguous with kamacite or apparently isolated from kamacite. Zoned taenite grains also exhibit dark-etching "cloudy zone" interiors which consist of submicron intergrowths of tetrataenite, antitaenite (a low moment phase), and martensite (Figs. 2–6) (Yang et al. 1997; Rancourt et al. 1999). Taenite grains in H and L chondrites occasionally contain martensite cores (Fig. 5a), but taenite grains in LL chondrites do not.

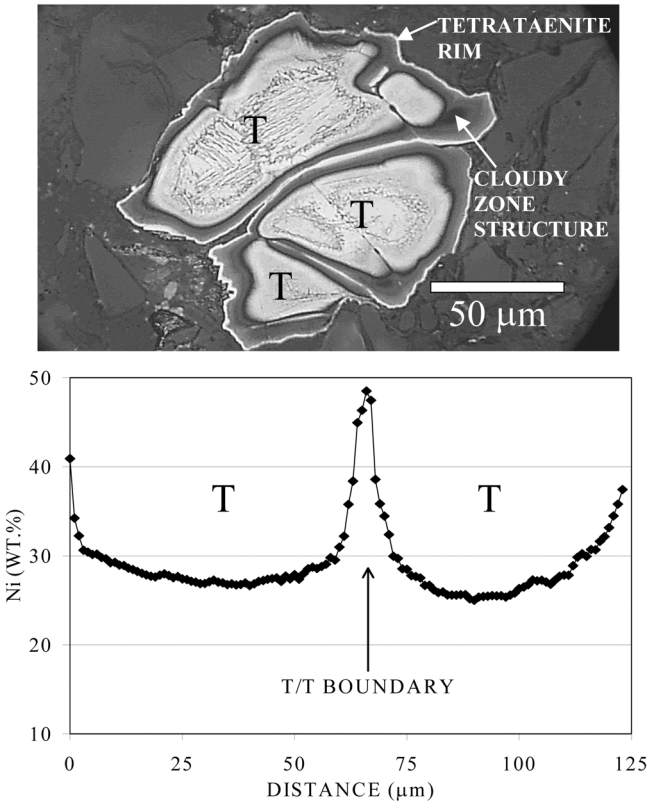

Fig. 5. a) Polycrystalline taenite particle in Allegan (H5). Three well-defined taenite grains (T) are delineated by tetrataenite rims and contain cloudy zone interiors. The largest taenite grains contain martensite (α_2) at their cores; b) electron microprobe Ni traverse across a taenite/taenite boundary. Each taenite grain displays a separate "M"-shaped Ni profile.

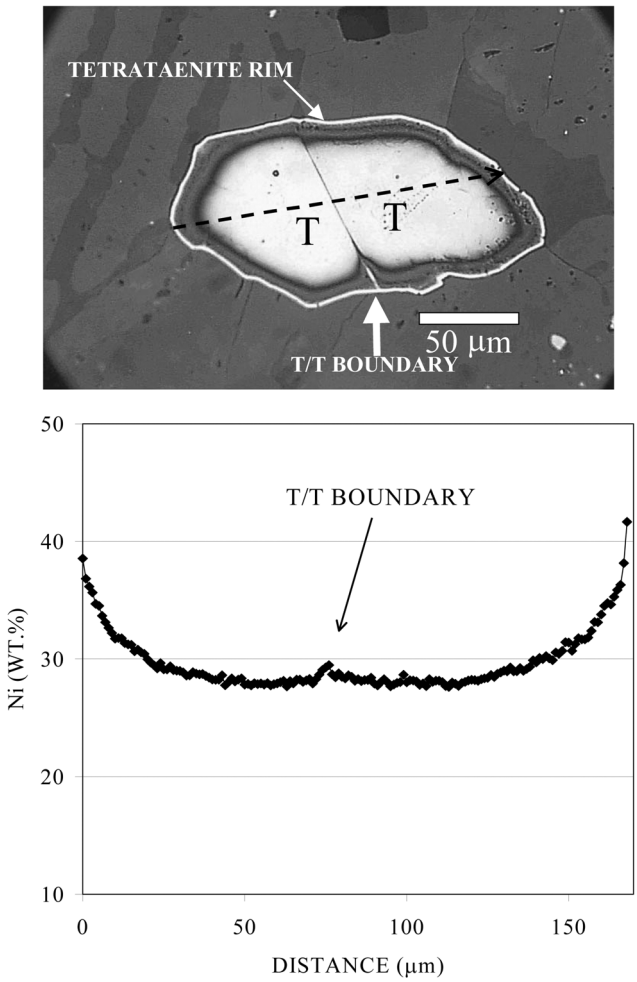

Fig. 6. a) Polycrystalline taenite particle in Kernouve (H6). Two taenite grains (T) are present but are poorly defined because the taenite/taenite boundary is not completely delineated by a tetrataenite rim. Note that the tetrataenite rim present at taenite/silicate interfaces pinches into the taenite particle along the internal taenite/taenite boundary (white arrow); b) microprobe Ni traverse across the taenite/taenite boundary. Taenite Ni concentrations are slightly elevated at the taenite/taenite boundary.

In the plane of sectioning, taenite may appear monocrystalline (Figs. 2 and 3) or polycrystalline (Figs. 4–6). The average taenite grain size in polycrystalline taenite increases through the type 4 → 6 petrographic sequence (Bevan 1983). In addition, taenite/taenite boundaries become less abundant, more poorly defined, and straighter as the petrographic type increases (Bevan 1983). Taenite grain boundaries are well-defined in type 4 and 5 ordinary chondrites because tetrataenite rims continue along the internal taenite grain boundaries (Fig. 5a). These well-defined taenite grain boundaries are interpreted to be relatively high angle grain boundaries (>5°) that etch deeply. Taenite grain boundaries tend to be more subtle in type 6 ordinary chondrites because their positions are not completely marked by tetrataenite rims (Fig. 6). In type 6 ordinary chondrites, tetrataenite rims commonly "pinch" into zoned taenite interiors at places where taenite grain boundaries intersect the taenite surface (Fig. 6). The poorly defined taenite grain boundaries are interpreted to be low angle grain boundaries (≤5°) that resist deep etching.

A "M"-shaped Ni profile with approximately 50 wt% Ni at the tetrataenite rim and 20–40 wt% Ni at the taenite core is observed in rim-to-rim microprobe traverses across zoned taenite (Figs. 2, 5, and 6). The tetrataenite rim composition does not depend on whether taenite is bordered by kamacite, silicate, or troilite. In polycrystalline taenite with well-defined taenite grains, each taenite grain exhibits a distinct "M"-shaped Ni profile (Fig. 5). When the taenite grains are poorly defined, taenite Ni profiles are only slightly elevated at taenite/taenite boundaries (Fig. 6). Taenite Co and P concentrations are below the microprobe detection limit of 0.05 and 0.02 wt%, respectively (detection limits are given at the 99% confidence level).

The kamacite in ordinary chondrites is usually polycrystalline. Shock-generated Neumann bands indicative of shock pressures between 1 and 13 GPa (Buchwald 1975) are commonly present. In Guarena (H6) the Neumann bands are discontinuous, suggesting that the metal particles experienced partial annealing after a shock event. In

Conquista (H4), Innisfree (L5), and Saratov (L4), the Neumann bands are curved, suggesting that plastic deformation followed the shock process.

Kamacite Ni concentrations always increase from rim (4.0–6.5 wt%) to core (5.5–7.0 wt%), a Ni distribution known as the Agrell effect (Agrell et al. 1963). Kamacite rim compositions do not depend on whether kamacite is bordered by taenite, silicate, or troilite. In polycrystalline kamacite, each kamacite grain exhibits its own Ni zoning profile. Kamacite Co concentrations vary systematically with respect to chondrite chemical group. Kamacite in H, L, and LL group chondrites contain 0.4–0.5, 0.7–1, and 1.5–3 wt% Co, respectively. These measurements are similar to kamacite composition data reported by Rubin (1990). Kamacite P concentrations are below the microprobe detection limit of 0.02 wt%.

Metallography of Zoneless Plessite Particles

Occurrence, Shapes, and Sizes of Zoneless Plessite Particles

Zoneless plessite particles occur in all of the H5–6 and L5–6 chondrites examined in this study (Table 1). The H4 and L4 chondrites contain small metal particles (<5 μm across) that appear to be zoneless plessite particles under an optical microscope. Unfortunately, these metal particles are too small for detailed microprobe studies. No zoneless plessite particles were observed in any of the LL chondrites examined in this study.

Zoneless plessite particles are more abundant in type 6 than in type 5 ordinary chondrites. In H6 chondrites Guarena, Kernouve, and Portales Valley, zoneless plessite particles comprise a larger fraction of the total metal than zoned taenite (Fig. 7). Bevan (1983) and Hutchison and Bevan (1983) made the same observation for metal in Kerouve (H6). Zoneless plessite particles occur in close proximity to zoned taenite + kamacite particles (Fig. 2), but sequential polishing experiments conducted in this study and by Willis and Goldstein (1983) revealed that zoneless plessite particles are always physically isolated from zoned taenite + kamacite particles. Ordinary chondrites that contain zoneless plessite particles have well-recrystallized textures, and the zoneless plessite particles usually occur locked between recrystallized silicate crystals. Some zoneless plessite particles occur partly or completely inside relict silicate chondrules or silicate clasts that may have been derived from chondrules (Sears and Axon 1975; Bevan 1983; Hutchison and Bevan 1983). Occasionally, zoned taenite + kamacite particles and zoneless plessite particles coexist within the same silicate clast.

Zoneless plessite particles have simple spherical or ellipsoidal shapes. In contrast to zoned taenite and kamacite, zoneless plessite particles are remarkably free from silicate, troilite, or chromite inclusions. However, zoneless plessite particles may be contiguous with small, 1–10 μm troilite or chromite grains.

Table 2 reports the apparent diameters of zoneless plessite particles in several ordinary chondrites. The sizes, however, are

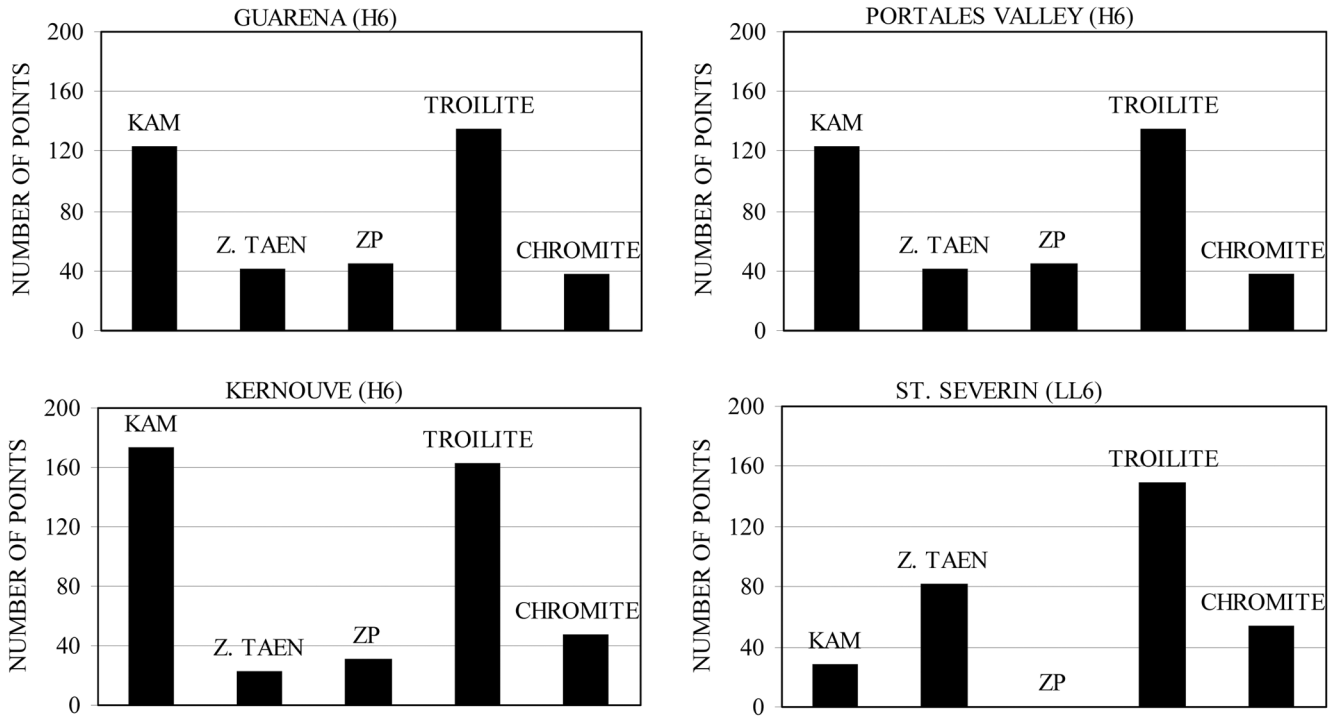

Fig. 7. Histograms showing the relative proportions of opaque particles in 4 ordinary chondrites. KAM, Z. TAEN, and ZP represent kamacite, zoned taenite, and zoneless plessite, respectively.

Table 2. Diameters of zoneless plessite particles in several ordinary chondrites.

Chondrite	Class	Diameter range (μm)	Average diameter (μm)	# Particles measured
Allegan	H5	16–79	33	9
Nuevo Mercurio	H5	17–68	37	12
Portales Valley	H6	20–100	54	20
Kernouve	H6	29–125	56	11
Estacado	H6	58–208	92	10
Guarena	H6	52–187	102	13
Barwell	L6	10–60	31	14
Elenovka	L6	28–91	56	5

biased in favor of large zoneless plessite particles that are easy to recognize. Zoneless plessite particles are generally <100 μm across, much smaller than zoned taenite + kamacite particles, which may be up to 1 mm across. The zoneless plessite particles that occur in type 6 ordinary chondrites are generally larger than those that occur in type 5 ordinary chondrites (Table 2).

Microstructure of Zoneless Plessite Particles

After Nital etching, zoneless plessite particles commonly appear relatively dark through an optical microscope (Figs. 2a and 8, right hand side). Scanning electron microscopy of etched zoneless plessite particles show that they consist of micron-sized tetrataenite precipitates within a kamacite matrix (Figs. 9 and 10; Table 3).[1] Zoneless plessite particles, unlike zoned taenite particles, do not have clear-etching tetrataenite rims or cloudy zone interiors.

The coarseness of a zoneless plessite particle microstructure varies from one particle to another within a given ordinary chondrite (Fig. 8). Fine-grained zoneless plessite particles contain tetrataenite plates that are crystallographically oriented within kamacite matrix (Fig. 9). Individual tetrataenite plates commonly extend across a zoneless plessite particle (Fig. 9). Some zoneless plessite particles have more coarse microstructures and appear brighter under an optical microscope (Fig. 8, left). Coarse-grained zoneless plessite particles are composed of tetrataenite blocks (up to 5 μm across) that lie within a kamacite matrix (Fig. 10; Table 3).

Within a given chondrite, zoneless plessite particle microstructures tend to coarsen as the particle size increases (Fig. 8). The zoneless plessite particles in Barwell (L5) and Elenovka (L5) have significantly finer microstructures than the zoneless plessite particles in H chondrites.

The kamacite matrix in zoneless plessite particles is composed of equi-dimensional kamacite grains that are 5–10 μm across (Fig. 10). The kamacite grain boundaries etch lightly and appear to be sub-boundaries that formed by recrystallization. Curved tetrataenite precipitates occasionally occur along kamacite grain boundaries.

[1]Hutchison and Bevan (1983) called the precipaitate phase in zoneless plessite particles "taenite." The precipitates contain approximately 50 wt% Ni—the composition of tetrataenite. Optical anisotropy is not observed due to the small precipitate sizes.

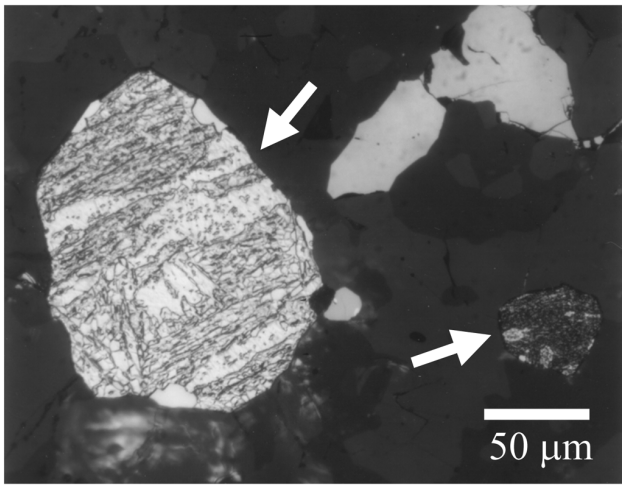

Fig. 8. Optical micrograph of Guarena (H6) showing a coarse-grained, bright-etching, zoneless plessite particle (left) and a fine-grained, dark-etching, zoneless plessite particle (right). In general, large zoneless plessite particles have coarse microstructures, while small zoneless plessite particles have fine microstructures.

Table 3. Compositions of metallic phases in the Kernouve (H6) zoneless plessite particle shown in Fig. 10. Positions 1–3 are tetrataenite, and positions 4–6 are kamacite.

Position	Fe (wt%)	Ni (wt%)	Co (wt%)	Total
1	47.4	52.2	0.02	99.6
2	48.1	51.9	0.00	100.0
3	47.7	51.7	0.00	99.4
4	96.6	3.3	0.57	100.4
5	95.3	4.0	0.51	99.9
6	95.4	3.5	0.55	99.5

Phase Compositions in Zoneless Plessite Particles

A microprobe point traverse across a zoneless plessite particle produces a saw-tooth-shaped Ni profile, with peaks and valleys corresponding to tetrataenite and kamacite respectively (Figs. 2 and 9). The tetrataenite and kamacite regions are usually smaller than the X-ray spatial resolution of ~1 μm. Therefore, the electron interaction volume overlaps tetrataenite and kamacite, and an average composition is obtained. Tetrataenite and kamacite are occasionally large enough for accurate microprobe analysis (i.e., Fig. 10). Figure 11 shows the Ni and Co concentrations of coexisting tetrataenite and kamacite in Guarena (H6), Kernouve (H6), Barwell (L5), and

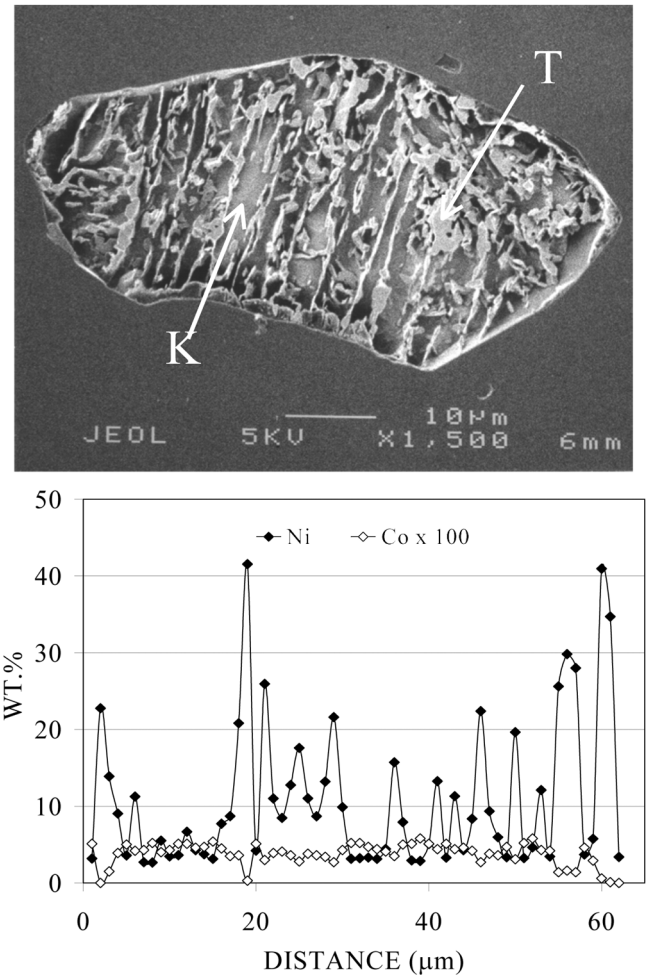

Fig. 9. a) Secondary electron image of a fine-grained zoneless plessite particle in Kernouve (H6). Tetrataenite plates (T) are aligned within the kamacite matrix (K). Many tetrataenite plates extend almost completely across the zoneless plessite particle. The kamacite matrix contains many small, equi-dimensional kamacite grains that are not visible in this micrograph; b) electron microprobe Ni and Co traverses across the zoneless plessite particle (traversed from left to right). Tetrataenite and kamacite regions are usually too small to resolve with an electron microprobe. Ni and Co are oppositely correlated.

Elenovka (L5). The tetrataenite precipitates contain 50–53 wt% Ni and the kamacite matrix contains 2.5–3.5 wt% Ni. The tetrataenite is essentially Co-free, but kamacite in H and L chondrites contains 0.4–0.6 wt% Co and 0.6–1.0 wt% Co, respectively. In Guarena (H6) and Elenovka (L5), tie-lines connecting tetrataenite and kamacite pass near the chondrite bulk metal compositions calculated from wet chemical data (Jarosewich 1990). Jarosewich (1990) did not report wet chemical analyses of Kernouve (H6) and Barwell (L5). Note, however, that the tie-lines connecting tetrataenite and kamacite pass through or near the average bulk metal composition of the corresponding chemical group (Fig. 11). Tetrataenite and kamacite compositions are easier to resolve in H chondrite zoneless plessite particles than in L chondrite zoneless plessite particles because zoneless plessite particle microstructures are

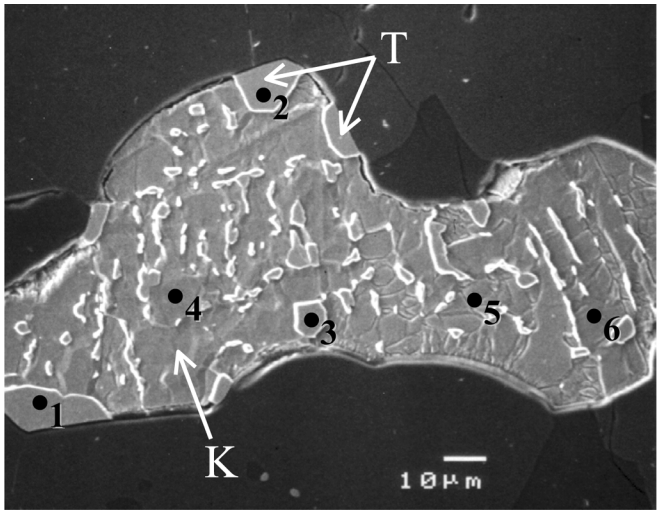

Fig. 10. Coarse-grained zoneless plessite particle in Kernouve (H6). Tetrataenite (T) occurs as blocks within kamacite (K) matrix. The numbers correspond to microprobe analyses reported in Table 3. Note that the kamacite matrix is composed of small, equi-dimensional grains.

more coarse in H chondrites. The tetrataenite and kamacite P concentrations in zoneless plessite particles are below the electron microprobe detection limit of 0.02 wt%.

Bulk Compositions of Zoneless Plessite Particles

The bulk compositions of individual zoneless plessite particles were measured by defocusing the electron microprobe beam to a diameter of 15–20 µm (Table 4). Each zoneless plessite particle was analyzed multiple times with the broadened beam, and the results were averaged to obtain an estimate of the particle's bulk composition. Zoneless plessite particles in H chondrites have bulk metal compositions of 9–11 wt% Ni and 0.4–0.5 wt% Co. Zoneless plessite particles in L chondrites have bulk metal compositions of 14–16 wt% Ni and 0.6–0.7 wt% Co. Table 4 shows that the bulk compositions of zoneless plessite particles (determined using broad beam electron probe microanalysis) are similar to the bulk metal compositions of the host chondrites (determined using wet chemical analysis). As described above, tie-lines connecting coexisting tetrataenite and kamacite in a zoneless plessite particle pass through or near the bulk metal composition of the host chondrite. This relationship provides additional evidence that zoneless plessite particle bulk compositions are the same as the bulk metal composition of the host chondrite.

DISCUSSION

Metal Particles During Prograde Metamorphism

Origin of Polycrystalline Taenite

The occurrence of clear-etching tetrataenite rims along taenite grain boundaries and "M"-shaped Ni profiles across

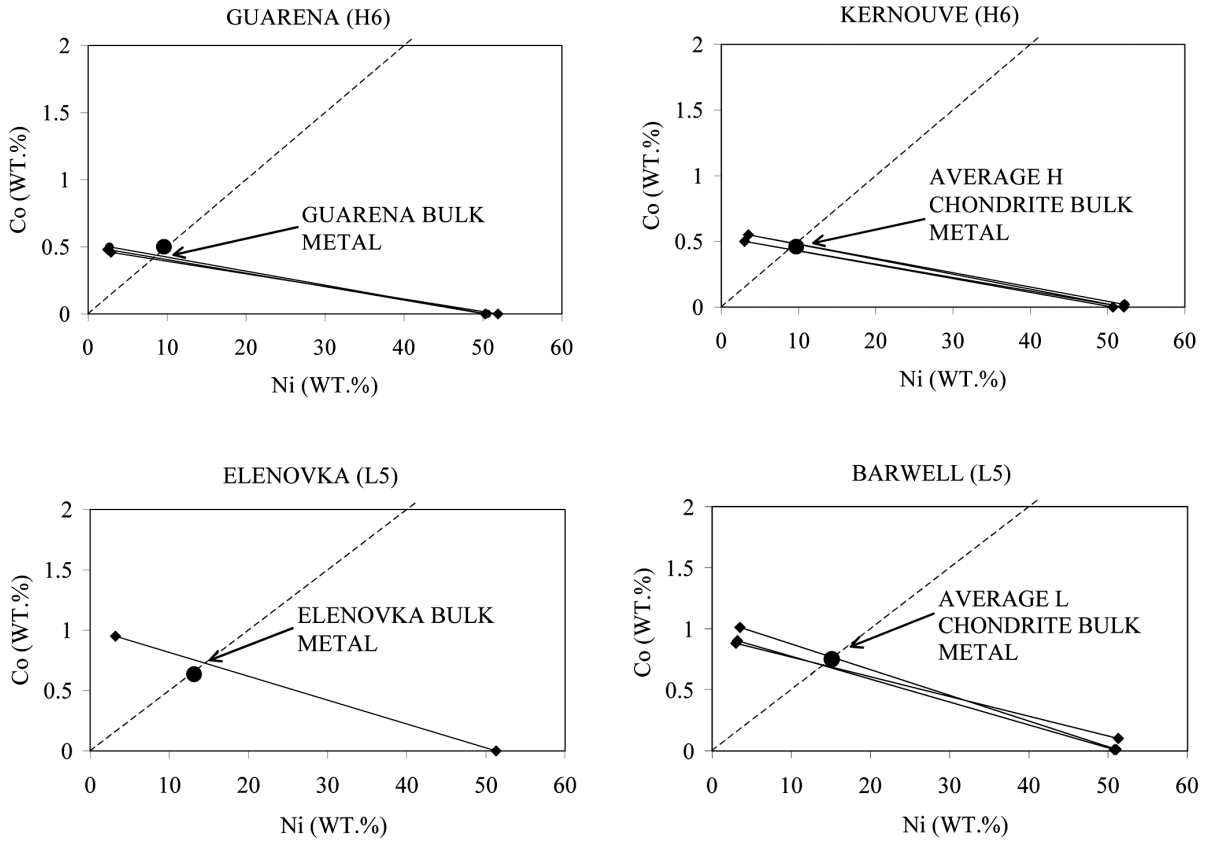

Fig. 11. Compositions of coexisting tetrataenite and kamacite in zoneless plessite particles. Tie-lines that connect coexisting tetrataenite and kamacite pass through or near the chondrite bulk metal compositions (filled circles). The dashed line represents the cosmic Co:Ni ratio of 1:20.

Table 4. Bulk compositions of individual zoneless plessite particles.[a]

	Kernouve (H6)			Guarena (H6)			Estacado (H6)			Barwell (L5)			Elenovka (L5)		
#[b]	Ni	Co	(n)[c]	Ni	Co	(n)[c]	Ni	Co	(n)[c]	Ni	Co	(n)[b]	Ni	Co	(n)[c]
1	9.4	0.45	(9)	10.2	0.42	(7)	9.4	0.42	(9)	14.9	0.63	6	14.8	0.64	14
2	10.2	0.44	(8)	9.6	0.48	(7)	10.1	0.40	(9)	14.4	0.61	14	14.2	0.61	14
3	10.8	0.51	(7)	11.2	0.42	(5)	9.9	0.42	(21)	15.7	0.68	9	14.9	0.60	11
4	9.5	0.44	(15)	9.7	0.40	(4)	10.9	0.34	(9)	16.0	0.68	13	15.5	0.66	10
5	10.1	0.46	(4)	10.0	0.46	(5)	9.1	0.40	(7)	14.9	0.65	14	15.3	0.64	3
6	8.9	0.46	(18)	10.2	0.44	(8)	10.9	0.42	(4)	–	–	–	–	–	–
7	10.1	0.44	(10)	9.4	0.44	(4)	11.1	0.43	(9)	–	–	–	–	–	–
8	9.9	0.46	(6)	10.4	0.46	(4)	11.2	0.44	(8)	–	–	–	–	–	–
9	9.1	0.46	(13)	11.2	0.38	(3)	10.0	0.45	(4)	–	–	–	–	–	–
10	9.6	0.44	(20)	10.0	0.37	(2)	10.3	0.40	(8)	–	–	–	–	–	–

[a]The bulk metal composition ranges in ordinary chondrites, determined by Jarosewich (1990) using wet chemical analysis, are as follows: H chondrites: 8.9–12.3 wt% Ni and 0.21–0.65 wt% Co; L chondrites: 12.0–22.0 wt% Ni and 0.42–1.13 wt% Co; LL chondrites: 25.4–53.5 wt% Ni and 0.86–2.58 wt% Co.
[b]Each # refers to a different zoneless plessite particle.
[c]The number of broad-beam analyses collected on each zoneless plessite particle is given by (n).

individual taenite grains (Fig. 5) clearly demonstrates that many taenite particles were polycrystalline at the time of kamacite precipitation. Polycrystalline taenite is proposed to be a relict solidification structure formed during fast chondrule cooling (Bevan 1983; Hutchison and Bevan 1983) or the result of impact-induced recrystallization (Scott and Rajan 1981). Polycrystalline taenite may have also formed during prograde metamorphism by sintering of metal in chondrules and in the matrix.

Taenite Grain Growth During Prograde Metamorphism

One might expect that taenite polycrystallinity in type 4–6 ordinary chondrites would be greatly reduced or eliminated by taenite grain growth during the long time scales available

during metamorphism. Indeed, the average taenite grain size increases through the type 4 → 6 petrographic sequence.

Taenite grain growth may have slowed or even stopped when the average taenite grain size approached the dimensions of the taenite particle because the taenite/taenite boundaries lacked curvature and could not migrate by surface tension forces (Reed-Hill 1964). Micron-sized particles of silicate, troilite, and chromite may have also exerted a drag force on migrating taenite/taenite boundaries, further impeding taenite grain growth. Therefore, taenite polycrystallinity most likely was preserved in type 4–6 ordinary chondrites in spite of annealing at 700–900°C for millions of years.

As discussed in a later section, many taenite particles in type 5 and 6 ordinary chondrites may have become single taenite crystals (monocrystalline) during prograde metamorphism. In a given ordinary chondrite, the smallest metal particles were most likely to become monocrystalline at peak metamorphic temperatures because the probability of containing taenite grain boundaries decreases as the metal particle size decreases.

Intragrain Metal Homogenization

The type 4–6 ordinary chondrites reached peak metamorphic temperatures of 700–900°C, where the stable metal phase is taenite (Fig. 1). Diffusion of Ni and Co will lead to chemical homogenization of each crystal of taenite whether the metal particle itself is monocrystalline or polycrystalline. The maximum taenite grain size expected to homogenize during a 1 Ma isothermal heat treatment, for example, was calculated using the relationship $x = (Dt)^{1/2}$, where x is distance, D is the Fe-Ni diffusion coefficient, and t is time. Using taenite Fe-Ni diffusion coefficients (Hopfe and Goldstein 2001), diffusion distances are 10, 2, and 0.4 mm at 900, 800, and 700°C, respectively. Therefore, chondritic metal particles, which are generally <1 mm across, should have homogenized with respect to Ni at peak metamorphic temperatures.

Bulk Compositions of Parent Taenite Particles

As shown in Fig. 1, metal particles in type 4–6 ordinary chondrites lie within the single phase taenite field at peak metamorphic temperatures of 700–900°C. We call these taenite particles "parent taenite particles," as they exist before cooling in their parent body.

Reconstructing the bulk composition of a parent taenite particle after it has decomposed to form a zoned taenite + kamacite particle is difficult. In principle, the parent taenite composition can be calculated if the final taenite composition, final kamacite composition, and final taenite:kamacite ratio are known. Unfortunately, taenite and kamacite compositions cannot be simply measured with an electron microprobe because each phase is chemically zoned. Moreover, the true taenite:kamacite ratio is rarely represented on the plane of sectioning because intergrowths between taenite, kamacite, silicates, and troilite have complex shapes.

When a taenite + kamacite particle cools, the equilibrium taenite Ni concentration increases along the taenite/(taenite + kamacite) solvus during cooling (Fig. 1). The original parent taenite composition may be preserved at or near the taenite grain core if the following special conditions are met: 1) the parent taenite grains must be relatively large (protecting taenite cores from taenite-kamacite equilibration); 2) the original taenite composition must be relatively Ni-rich (resulting in low kamacite precipitation temperatures where taenite volume diffusion is relatively slow); and 3) chondrite cooling rates must be relatively fast (limiting long-range volume diffusion).

The Hopfe and Goldstein (2001) metallographic cooling rate program was used to calculate the minimum taenite grain size required to preserve the parent taenite Ni concentration at taenite cores (to within 1 wt%). Calculations were made for parent taenite Ni concentrations of 10, 20, and 30 wt% and for various cooling rates. For H and L chondrites with metal Ni contents of ~10 and ~15 wt%, respectively (Fig. 1), taenite grains must be >500 to 1000 μm for cooling rates slower than 25°C/Ma (Table 1). Few taenite grains are of this size, and therefore, most taenite grains are too small to preserve the original taenite composition at taenite cores. For LL chondrites with metal Ni contents of ~30 wt% (Fig. 1), taenite grains must be >50 to 150 μm for the same cooling rate range. Many taenite grains in LL chondrites are large enough to preserve the original taenite composition at taenite cores. For example, large taenite grains in St. Severin (LL6) (250–500 μm across) contain 31.5 wt% Ni and 1.3 wt% Co at their cores. These taenite core compositions (measured with an electron microprobe) are very similar to the St. Severin bulk metal composition of 32 wt% Ni and 1.2 wt% Co determined using wet chemical techniques (Jarosewich 1990). This observation supports the idea that the parent taenite particles in ordinary chondrites were homogeneous from particle to particle at the beginning of cooling.

In contrast to zoned taenite + kamacite particles, the bulk compositions of zoneless plessite particles are relatively easy to measure using an electron microprobe. Different zoneless plessite particles in a given ordinary chondrite have bulk Ni and Co concentrations that are similar to each other and also similar to the bulk metal composition of the host chondrite (see Table 4). The compositional homogeneity among zoneless plessite particles provides additional evidence that all parent taenite particles in type 5–6 ordinary chondrites were the same composition at the beginning of cooling.

Intergrain Metal Homogenization

In primitive ordinary chondrites, such as Semarkona (LL3.0) and Krymka (LL3.1), chondrule and matrix metal particles have bulk compositions that vary from one particle to another; the bulk composition of a metal particle does not generally represent the bulk metal composition of the host chondrite. As discussed in the previous sections, the parent

taenite particles in highly equilibrated type 5 and 6 ordinary chondrites were homogeneous within and between taenite particles at peak metamorphic temperatures. Apparently, chondritic metal particles started out with widely varying compositions but chemically equilibrated with each other during metamorphic heating. Intergrain homogenization of metal particles through the type 3 → 6 petrographic sequence parallels the intergrain homogenization of olivine and pyroxene crystals that occurred through this sequence.

Intergrain olivine and pyroxene homogenization during prograde and peak-temperature metamorphism can be understood in terms of Fe-Mg volume diffusion because silicate minerals form a continuous network. Chondritic metal particles, on the other hand, are physically isolated from each other by intervening silicates. There are 2 reasonable mechanisms by which physically isolated metal particles could homogenize with each other during metamorphism: 1) metal-silicate equilibration (Reisener and Goldstein 2001); and 2) metal vapor transport along silicate grain boundaries (Reisener and Goldstein 1999b). These processes for atom transport are most effective at peak metamorphic temperatures and are of lesser importance during cooling.

Metal Particles During Cooling

We will consider the metallographic evolution of polycrystalline and monocrystalline taenite particles during cooling and will discuss a comprehensive model where polycrystalline taenite particles promote the formation of zoned taenite + kamacite particles during cooling and monocrystalline taenite particles promote the formation of zoneless plessite particles. The experimental basis for this discussion is given in a companion paper (Reisener and Goldstein 2003).

Formation of Zoned Taenite + Kamacite Particles from Polycrystalline Taenite

The formation of zoned taenite and kamacite in chondritic metal can be understood in terms of the taenite → taenite + kamacite reaction during slow cooling from the peak metamorphic temperature (Fig. 12, left hand side). Kamacite nucleation sites are difficult to identify in ordinary chondrites because kamacite has consumed large portions of the original taenite grains during growth at slow cooling rates. Fortunately, laboratory cooling experiments provide insight into the kamacite nucleation process in low-P alloys (Reisener and Goldstein 2003). We have shown experimentally that kamacite does not nucleate homogeneously from P-free taenite during continuous cooling; rather, kamacite nucleates heterogeneously at taenite/taenite grain boundaries (Reisener and Goldstein 2003). The kamacite grain boundary precipitates subsequently consume parent taenite grains (Fig. 12, left hand side) by a process that involves both grain boundary and volume diffusion (Reisener and Goldstein 2003).

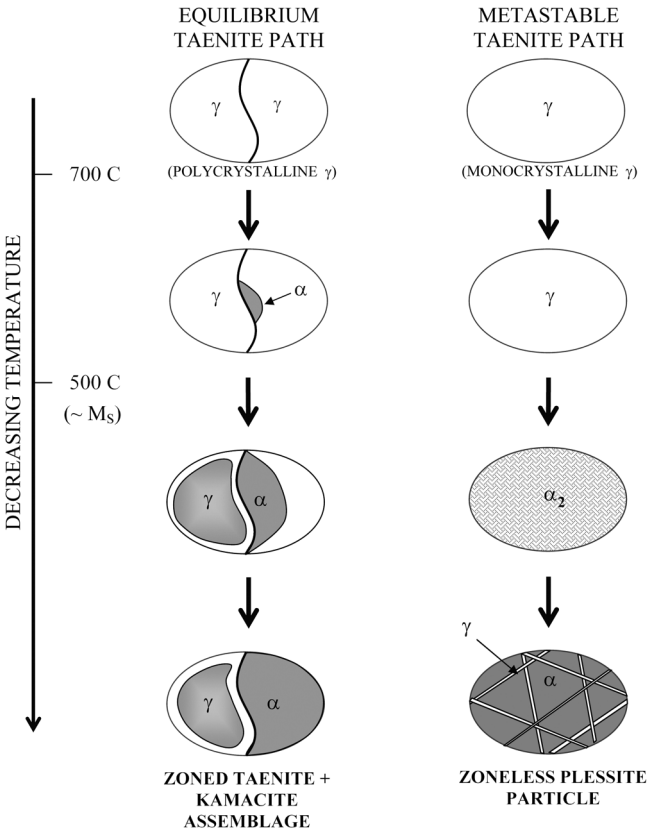

Fig. 12. Schematic showing the evolution of polycrystalline taenite (left) and monocrystalline taenite (right) during cooling. T, K, and α_2 represent taenite, kamacite, and martensite, respectively. M_s indicates the martensite start temperature for an Fe-10Ni alloy.

In ordinary chondrites, the final size of a kamacite precipitate was probably limited by the size of the taenite grain being consumed. The irregular shapes of many taenite/kamacite interfaces in ordinary chondrites probably reflect the irregular shapes of the taenite/taenite boundaries upon which nucleation occurred (Fig. 12, left hand side).

Taenite and kamacite maintained equilibrium at taenite/kamacite interfaces during cooling (line A–E in Fig. 1). The taenite Ni concentration at taenite/kamacite interfaces increases with decreasing temperature, and Ni diffusion slowed at low temperatures, causing the classic "M"-shaped Ni gradient to develop in taenite. Taenite-kamacite equilibrium was also maintained at metal/silicate and metal/troilite interfaces during cooling because Fe-Ni diffusion is much faster across metal surfaces than through metal lattices (Willis and Goldstein 1983; see Fig. 13). The fast metal surface diffusion rates enable Ni mobility so that taenite Ni gradients near taenite/kamacite interfaces are similar to taenite Ni gradients near taenite/silicate and taenite/troilite interfaces. The same process explains why kamacite Ni gradients at kamacite/taenite interfaces are similar to kamacite Ni gradients at kamacite/silicate and kamacite/troilite interfaces. In polycrystalline taenite with well-

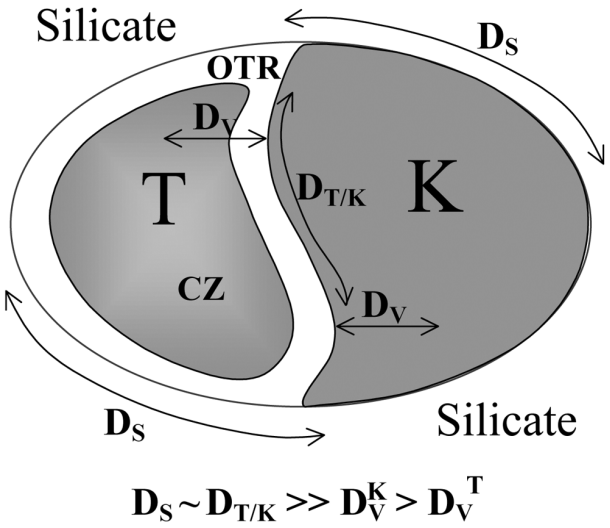

Fig. 13. Fe-Ni diffusion paths in a zoned taenite (T) + kamacite (K) particle. Diffusion occurs through the taenite and kamacite volumes (D_V), along taenite/kamacite interfaces ($D_{T/K}$), and along metal surfaces (D_S). In polycrystalline taenite and kamacite, diffusion also occurs along the internal grain boundaries. Diffusion along metal surfaces and taenite/kamacite interfaces is much faster than diffusion through taenite and kamacite volumes. OTR and CZ represent the zoned taenite outer taenite rim and cloudy zone, respectively.

developed taenite grains (high angle grain boundaries), rapid Fe-Ni diffusion along taenite/taenite boundaries increases Ni mobility and allows "M"-shaped Ni gradients to develop across each taenite grain (Reisener and Goldstein 2003). Grain boundary diffusion rates decrease as the temperature decreases but increase relative to volume diffusion rates as the temperature decreases (Shewmon 1989). Therefore, grain boundary diffusion becomes increasingly important during chondrite cooling.

The zoned taenite cloudy zone structure formed by spinodal decomposition at temperatures below ~400°C (Yang et al. 1997) and the cores of taenite grains (low Ni) in H and L chondrites occasionally transformed to martensite by a diffusionless transformation (Fig. 5a). On the other hand, taenite cores in LL chondrites were too Ni-rich (>30 wt%) to form martensite (see Fig. 1).

Wood (1967) proposed that physically isolated taenite and kamacite particles equilibrated with each other during cooling because Fe and Ni diffused rapidly through intervening silicates. However, sequential polishing of thick sections conducted in this study and by Willis and Goldstein (1983) demonstrate that taenite and kamacite are contiguous, touching each other in 3 dimensions. The isolated appearance of zoned taenite particles and kamacite particles is actually an artifact of viewing complex-shaped, 3-dimensional metal assemblages on a 2-dimensional surface. Therefore, fast Fe-Ni diffusion through silicates during cooling need not be considered in relation to the equilibration of taenite and kamacite phases.

Formation of Zoneless Plessite Particles from Monocrystalline Taenite

Any model for the formation of zoneless plessite particles must explain the following observations: 1) zoneless plessite particles and zoned taenite + kamacite particles are present within the same ordinary chondrite (they occasionally occur within the same silicate clast); 2) zoneless plessite is commonly a major component of the metal in a given ordinary chondrite; 3) zoneless plessite particles lack systematic rim-to-rim Ni zoning; 4) the abundance and sizes of zoneless plessite particles increase systematically with increasing petrographic type; and 5) the bulk compositions of zoneless plessite particles are the same as the bulk metal composition of the host chondrite.

The microstructures of chondritic zoneless plessite particles are very similar to the microstructures of plessitic tetrataenite + kamacite intergrowths in iron meteorites, which occur in the center of the "M"-shaped taenite Ni profiles. As discussed by Massalski et al. (1966), iron meteorite plessite formed by the taenite → martensite → taenite + kamacite reaction during slow cooling. The microstructural similarities of chondritic zoneless plessite to iron meteorite plessite suggest that zoneless plessite particles formed by the same reaction sequence during cooling.

The presence of martensite in ordinary chondrites is commonly regarded as conclusive evidence for fast metal cooling rates (e.g., Bevan 1983; Hutchison and Bevan 1983; Rubin 1990). This interpretation is based on a classic experimental study by Kaufman and Cohen (1956), which showed that Fe-Ni taenite transforms to martensite upon cooling at rates of 5°C/min or faster. The diffusion controlled taenite → taenite + kamacite reaction is suppressed during such fast cooling, forcing taenite to form martensite upon reaching the martensite start temperature. Indeed, fast chondrite cooling after shocking often produces martensite (Smith and Goldstein 1977; Bennett and McSween 1996).

Taenite is less well-recognized for its ability to transform to martensite even if the cooling rate is extremely slow. For example, zoned taenite regions in ordinary chondrites and iron meteorites commonly contain martensite cores (Fig. 5) even though these meteorites cooled at rates of 1–100°C/Ma. The martensite cores represent regions of taenite in which kamacite did not precipitate during cooling because heterogeneous nucleation sites were not present. The taenite cores remained metastable (Fe-supersaturated) during cooling through the taenite + kamacite field and transformed to martensite upon reaching the martensite start temperature (Massalski et al. 1966).

Fe-Ni alloy cooling experiments (discussed in Reisener and Goldstein [2003]) have shown that P-free taenite will precipitate kamacite only if high energy taenite grain boundaries are present (Reisener and Goldstein 2003). If taenite grain boundaries are absent, taenite will undercool to

temperatures below the martensite start temperature and transform to martensite by a diffusionless transformation.

We propose that monocrystalline parent taenite particles in slow-cooled ordinary chondrites undercooled below the taenite/(taenite + kamacite) solvus (Fig. 1) without forming kamacite because kamacite nucleation sites (taenite grain boundaries) were not present. The monocrystalline taenite particles remained homogeneous during cooling, transformed to martensite upon reaching the martensite-start temperature (Fig. 1), and finally decomposed to tetrataenite + kamacite plessite during subsequent cooling.

The right hand side of Fig. 12 illustrates the decomposition of a monocrystalline taenite particle to form a zoneless plessite particle during cooling. When a homogeneous monocrystalline taenite particle cools below the martensite start temperature (for example, ~500°C for an Fe-10Ni alloy), it transforms to martensite. The martensite subsequently decomposes by the martensite → tetrataenite + kamacite reaction at temperatures below ~320°C, the Fe-50Ni order/disorder transition temperature. Martensite decomposition is enhanced because: 1) numerous dislocations in martensite provide sites for heterogeneous nucleation of tetrataenite; and 2) martensite volume diffusion rates are much higher than taenite volume diffusion rates (Romig and Goldstein 1981). During the same cooling process, a polycrystalline taenite particle can transform to a zoned taenite + kamacite particle as shown on the left hand side of Fig. 12.

The observation that tetrataenite plates extend across a zoneless plessite particle (Fig. 9) provides strong evidence that zoneless plessite particles evolved from monocrystalline taenite particles. During the martensite decomposition process, the kamacite matrix recrystallizes into polycrystalline kamacite (Fig. 10), relieving the inherent strain of the martensite matrix. Curved tetrataenite precipitates occasionally lie along kamacite subboundaries, suggesting that some tetrataenite precipitation occurred during or after kamacite recrystallization.

Taenite silicate interfaces were not favorable sites for kamacite nucleation as originally proposed by Willis and Goldstein (1983). Otherwise, all parent taenite particles would have precipitated kamacite at taenite/silicate interfaces during cooling, and zoneless plessite particles would not have formed. Kamacite nucleation at taenite/silicate interfaces in low-P metal apparently does not lower the system energy enough to make precipitation feasible. Although kamacite nucleation at taenite/silicate interfaces reduces the taenite/silicate interfacial area, the nucleation process also introduces additional kamacite/silicate interfacial area. Therefore, no net reduction occurs in the metal/silicate interfacial area.[2] On the other hand, kamacite nucleation at taenite/taenite boundaries is energetically favorable because a taenite/kamacite interface has less energy than a taenite/taenite interface (Aaron and Aaronson 1968).

That zoneless plessite particles increase in size and abundance with increasing petrographic type (Table 2) is entirely consistent with the formation mechanism described above. Taenite grain coarsening was most extensive in type 6 ordinary chondrites because these meteorites reached the highest metamorphic temperatures. Therefore, monocrystalline taenite particles were the largest and most abundant in type 6 ordinary chondrites.

Other Models for the Formation of Zoneless Plessite Particles

The formation of zoneless plessite particles from slow cooled monocrystalline parent taenite particles is consistent with the 5 microstructural and microchemical observations discussed in the previous section. Other models for zoneless plessite particle formation have been proposed and are discussed in the following sections.

Hot Accretion-Autometamorphism

Bevan (1983) and Hutchison and Bevan (1983) observed that some zoneless plessite particles occur inside relict silicate chondrules. They inferred from this textural setting that zoneless plessite particles formed during chondrule solidification and subsequent solid-state cooling. According to their model, the diffusion-controlled taenite → taenite + kamacite reaction was suppressed in chondrule metal due to fast chondrule cooling rates. The homogeneous but metastable (Fe-supersaturated) parent taenite particles cooled rapidly through the taenite + kamacite field and transformed to homogeneous martensite upon reaching the martensite start temperature. Bevan (1983) and Hutchison and Bevan (1983) further postulated that chondrule cooling rates decreased at temperatures below the martensite start temperature, allowing martensite to decompose to more stable tetrataenite + kamacite plessite.

Bevan (1983) and Hutchison and Bevan (1983) suggested that the presence of zoneless plessite particles in ordinary chondrites precludes the possibility that ordinary chondrites experienced metamorphic heating into the single-phase taenite field. Such metamorphic heating, they argued, would have destroyed zoneless plessite particle microstructures. They concluded that ordinary chondrites aggregated while the chondrules were hot and experienced "autometamorphism" during post-accretionary cooling.

The hot accretion-autometamorphism model for zoneless plessite particle formation has several shortcomings. First, most zoneless plessite particles occur outside recognizable relict silicate chondrules. The strongly recrystallized textures between zoneless plessite particles and the surrounding silicate crystals are more consistent with a metamorphic

[2]Kamacite nucleation at taenite/silicate interfaces may be important in P-saturated alloys as demonstrated by the common occurrence of swathing kamacite around olivine crystals in pallasites. In the pallasites, phosphides commonly occur at metal/olivine interfaces and play a role in the nucleation of swathing kamacite around the olivine inclusions (Buchwald 1975).

origin. Second, if zoneless plessite particles formed during chondrule formation, they (or their martensite precursors) should be best preserved in type 3 and 4 ordinary chondrites. However, zoneless plessite particles and martensite particles are rare or absent in type 3 and 4 ordinary chondrites.[3] The tendency for the number and sizes of zoneless plessite particles to increase with increasing petrographic type implies that these metal particles have a metamorphic origin. The hot accretion-autometamorphism model also fails to explain how zoneless plessite particles (which supposedly formed at fast cooling rates) and zoned taenite + kamacite particles (which formed at cooling rates on the order of 1–100°C/Ma; Wood [1967]; Willis and Goldstein [1981]) came to coexist within the same ordinary chondrite.

Post-Metamorphic Brecciation

Rubin (1990) and Rubin and Brearley (1996) proposed that zoneless plessite particles are aberrant metal particles that were incorporated into ordinary chondrites during low temperature brecciation events. These workers postulate that zoneless plessite particles evolved separately from zoned taenite + kamacite particles, and were formed by shock-homogenization (producing homogeneous taenite) followed by rapid cooling to temperatures below the martensite start temperature (producing homogeneous martensite). Through a brecciation process, the homogeneous martensite particles were subsequently incorporated into ordinary chondrites that already contained zoned taenite + kamacite particles that formed during slow cooling. Finally, the aberrant martensite particles decomposed to form tetrataenite + kamacite plessite without systematic zoning. Chondrite brecciation must have occurred at temperatures below the taenite/(taenite + kamacite) solvus to preserve zoneless plessite microstructures. The post-metamorphic breccias were presumably lithified by shock-melting along crystal boundaries rather than by high temperature sintering (Rubin 1990).

Many ordinary chondrites are well-known to have become brecciated during or after cooling from peak metamorphic temperatures (Scott and Rajan 1981; Scott et al. 1985). Post-metamorphic breccias are commonly characterized by angular (texturally unequilibrated) silicate clasts that may be compositionally different from other silicates in the same chondrite. Also, taenite particles in post-metamorphic breccias commonly exhibit incoherent metallographic cooling rates, indicating that the zoned taenite + kamacite particles cooled in diverse geologic environments before chondrite aggregation (Scott and Rajan 1981).

The ordinary chondrites examined in this study lack brecciated textures. Silicate clasts that occasionally host zoneless plessite particles are compositionally identical to the surrounding silicate crystals, implying that the silicate clasts (and included zoneless plessite particles) equilibrated in situ. The metallographic cooling rates of the ordinary chondrites in this study, when available, are coherent (1 value), suggesting that all zoned taenite + kamacite particles formed in situ (Table 1). The occasional presence of a zoneless plessite particle and a zoned taenite + kamacite particle within the same silicate clast provides excellent evidence that both types of metal particles had identical thermal histories. The post-metamorphic brecciation model does not explain why zoneless plessite particles become larger and more abundant with increasing petrographic type. The post-metamorphic brecciation model also fails to explain how zoneless plessite particles came to have bulk compositions that are similar to the bulk metal composition of the host chondrite.

Shock Processing In Situ

A shock-metamorphic origin for zoneless plessite particles requires a complex thermal history. First, parent taenite particles must have experienced slow cooling from peak metamorphic temperatures to low temperatures, resulting in the formation of zoned taenite + kamacite particles. Second, a transient shock event must have caused shock-heating/homogenization of some zoned taenite + kamacite particles while leaving others unaltered. The shock-heated metal particles may have reached temperatures within the single-phase taenite field where solid-state homogenization occurred (Wood 1967). Alternatively, the shock-heated metal may have reached liquidus temperatures where melting and liquid-state homogenization occurred (Smith and Goldstein 1977). Third, shock-homogenized taenite particles must have cooled rapidly to temperatures below the martensite start temperature to suppress kamacite precipitation. Finally, the homogeneous martensite particles must have cooled more slowly at lower temperatures (or have experienced reheating within the taenite + kamacite field), resulting in martensite decomposition. The final metal microstructure would be an unzoned, tetrataenite + kamacite plessite particle. Post-shock residual temperatures must have been below ~500°C to preserve some of the original zoned taenite + kamacite particles. The low post-shock residual temperatures also allowed shock-homogenized taenite particles to cool rapidly to the martensite start temperature.

Several aspects of the shock-metamorphism model for zoneless plessite particle formation are problematic. For example, explaining why some zoned taenite + kamacite particles became completely homogenized during shock heating, while nearby zoned taenite + kamacite particles were undisturbed, is difficult. That steep temperature gradients could be maintained for the time scales required for solid-

[3] Silicate chondrules in Semarkona (LL3.0) and Krymka (LL3.1) contain small metal particles composed of tetrataenite + kamacite plessite. These plessitic metal particles are much smaller than zoneless plessite particles in equilibrated ordinary chondrites and have compositions that differ significantly from the bulk metal composition of the host chondrite. The chondrule metal microstructures in these very primitive chondrites formed by the taenite → martensite reaction during fast chondrule cooling followed by the martensite → tetrataenite + kamacite reaction during mild metamorphic heating (e.g., Reisener et al. 1999a).

state metal homogenization is unlikely. Typically, shock-reheated taenite particles partially preserve the original "M"-shaped taenite Ni profiles because solid-state homogenization was incomplete (Smith and Goldstein 1977).

Also, that zoneless plessite particles were shock-homogenized at igneous temperatures is unlikely. Shock-melted and rapidly solidified metal particles form dendritic textures with steep Ni gradients due to nonequilibrium solidification (Smith and Goldstein 1977; Scott 1982). Zoneless plessite particles, however, do not exhibit such systematic Ni zoning.

Chondritic metal particles that have been severely shock heated commonly contain >0.1 wt% P due to P reduction from phosphates at high temperatures (Smith and Goldstein 1977). The P concentrations of chondritic zoneless plessite particles, however, are below the electron microprobe detection limit of 0.02 wt%.

Olivine and orthopyroxene crystals in highly shocked ordinary chondrites display undulatory extinction due to lattice straining and fracturing due to brittle deformation. Shocked olivine crystals commonly contain elevated CaO concentrations due to CaO partitioning from orthopyroxene and retention of CaO upon rapid cooling (Stöffler et al. 1991). We observed that olivine and orthopyroxene crystals that are adjacent to zoneless plessite particles have sharp optical extinction, lack significant fracturing, and have normal CaO concentrations (<0.06 wt%).

Other Models Summary

The occurrence of zoneless plessite particles in ordinary chondrites, and the metallographic characteristics of these particles, cannot be explained in terms of hot accretion-autometamorphism, post-metamorphic brecciation, or shock-processing. The new model for metal particle evolution (described above) maintains that zoned and unzoned metal particles can develop during the same cooling process in the same ordinary chondrite. Two parent taenite particles with identical chemical compositions but different structures (polycrystalline versus monocrystalline) can experience the same cooling history but undergo different reaction paths during cooling (Fig. 12). The result is 2 different metal microstructures (zoned taenite + kamacite particles and zoneless plessite particles) within the same ordinary chondrite (see Fig. 2).

Microstructural Variations Among Zoneless Plessite Particles

The microstructures of zoneless plessite particles vary from one particle to another within a given ordinary chondrite (Fig. 8). Bevan (1983) and Hutchison and Bevan (1983) attributed these microstructural variations to variations in zoneless plessite particle bulk compositions. However, these compositions are essentially the same within a given chondrite and are approximately equal to the bulk metal composition of the host chondrite (Table 4).

Interestingly, the coarseness of a zoneless plessite structure increases as the size of the particle increases (Fig. 8). The effect of taenite particle size on the Fe-Ni martensite start temperature was investigated experimentally by Turnbull (1955). Upon cooling monocrystalline taenite particles that were 37–100 μm in diameter, Turnbull (1955) observed that the effective martensite start temperature decreased systematically as the taenite particle size decreased. The lower martensite start temperatures of small taenite particles has been attributed to a statistically smaller defect population that promotes martensite nucleation (Turnbull 1955; Kachi et al. 1962). The small taenite particles also contain few dislocations that accommodate plastic deformation during martensite formation (Kajiwara et al. 1987; Zhou et al. 1990; Zhou et al. 1991; Kajiwara et al. 1991). The largest monocrystalline taenite particles in ordinary chondrites probably transformed to martensite at temperatures near the martensite start temperature; the martensite decomposed at relatively high temperatures and produced relatively coarse plessite structures (Fig. 8). Smaller monocrystalline taenite particles probably transformed to martensite at temperatures well below the martensite start temperature; the martensite decomposed at lower temperatures and produced finer plessite structures (Fig. 8).

The microstructural variations among zoneless plessite particles from different ordinary chondrites can be attributed to bulk metal composition variations as originally suggested by Bevan (1983) and Hutchison and Bevan (1983). The parent taenite particles in L chondrites are Ni-rich relative to the parent taenite particles in H chondrites and, therefore, have lower martensite start temperatures (Fig. 1). The lower martensite formation/decomposition temperatures in L chondrites produced finer zoneless plessite particle microstructures.

Absence of Zoneless Plessite Particles in LL Group Chondrites

The absence of zoneless plessite particles in LL group chondrites can be explained, in part, by the relatively Ni-rich bulk metal compositions of >30 wt% Ni in these chondrites (Fig. 1). Such Ni-rich taenite does not form plessite because the martensite start line is crossed at a temperature below room temperature during cooling (Fig. 1). Martensite formed at such a low temperature can not decompose to equilibrium tetrataenite + kamacite due to the low volume diffusion rates.

On the other hand, our model postulates that kamacite will not precipitate in monocrystalline taenite particles in LL chondrites during cooling, and the taenite phase will remain homogeneous throughout the cooling process. Such Ni-rich, homogeneous taenite particles are expected to form a cloudy zone structure by the process of spinodal decomposition at

temperatures below 300°C (Fig. 1). Metallographic studies of the 3 LL chondrites examined in this study failed to reveal the presence of chemically homogeneous taenite particles composed entirely of a cloudy zone structure. Unfortunately, relatively few metal particles were available for study in these metal-poor chondrites.

Formation of Widmanstätten Structure in Portales Valley (H6) and Other Ordinary Chondrites

In Reisener and Goldstein (2003), Part 1 of this study, we used Fe-Ni alloy cooling experiments to investigate the taenite decomposition process during cooling. The cooling experiments demonstrate that kamacite will precipitate, in P-free taenite, at taenite/taenite and possibly at taenite/FeS interfaces during cooling. On the other hand, Widmanstätten-type kamacite plates will precipitate within P-containing taenite grains. These experimental results are consistent with meteorite metallography: Widmantätten structure is absent from ordinary chondrite metal (P-poor) but is ubiquitous in iron meteorite metal (P-bearing).

Portales Valley (H6) is an interesting ordinary chondrite because it contains metallic veins with a well-developed Widmanstätten structure. The metal in this chondrite contains 0.01 wt% P (Alex Ruzicka, personal communication). This P concentration is low compared to P concentrations in iron meteorites (up to 2 wt% P). However this P content is 5 times higher than metal P concentrations measured in typical ordinary chondrites (<0.002 wt%; Reed 1964). The metallography of Portales Valley may indicate that P concentrations as low as 0.01 wt% promote the formation of a Widmanstätten structure. Alternatively, the metal P concentrations in Portales Valley may have been higher than 0.01 wt% at the time the Widmanstätten structure formed. Goldstein and Smith (1977) showed that chondritic metal particles that have been severely shock heated commonly contain >0.1 wt% P due to P reduction from phosphates at high temperatures. If the metal veins in Portales Valley formed by impact-induced melting, as proposed by Rubin et al. (2001), the metal veins may have become P-enriched relative to metal particles in the silicate fraction. The high P concentrations in metallic veins may have promoted the development of a Widmanstätten structure during cooling. At low temperatures, P must have been oxidized from metal and incorporated into phosphates during the cooling process, leaving the metallic veins with ~0.01 wt% P. This later scenario is consistent with the observation that phosphates are commonly associated with metallic veins in Portales Valley.

Ordinary chondrite metal particles typically exhibit irregular taenite/kamacite interfaces (Fig. 3). However, crude Widmanstätten structures are occasionally observed (Fig. 4). Although non-crystallographic in appearance, irregularly shaped taenite/kamacite boundaries exhibit a Widmanstätten-type crystallographic orientation in which kamacite is oriented along the taenite octahedral planes (see Reisener and Goldstein 2003). The metal particles in ordinary chondrites may form a crude Widmanstätten structure if the taenite/taenite boundary (upon which kamacite nucleation occurs) is oriented roughly along a taenite octahedral plane.

Kamacite Ni and Co Compositions in Ordinary Chondrites

Usually, we assume that all kamacite grains in ordinary chondrites formed by the diffusion controlled taenite → taenite + kamacite transformation during cooling from peak metamorphic temperatures. The present study, however, has shown that chondritic kamacite formed by 2 fundamentally different mechanisms (see Fig. 12).

Kamacite Ni concentrations depend on the mechanism and temperature of kamacite formation. The kamacite grains in zoned taenite + kamacite particles, which formed by the diffusion controlled reaction taenite → taenite + kamacite (Fig. 12), contain 5.0–7.0 wt% Ni at the cores and 4.0–6.5 wt% Ni at the rims. The kamacite rim Ni concentrations correspond to kamacite-taenite closure temperatures between 450 and 200°C (Hopfe and Goldstein 2001).

Kamacite grains in zoneless plessite particles, which formed by the reaction taenite → martensite → tetrataenite + kamacite (Fig. 12), contain 2.5–3.5 wt% Ni, corresponding to kamacite-tetrataenite closure temperatures below 200°C (Hopfe and Goldstein 2001). Kamacite in zoneless plessite particles formed and/or equilibrated at lower temperatures than kamacite in zoned taenite + kamacite particles because martensite volume diffusion rates are much faster than taenite volume diffusion rates (Romig and Goldstein 1981).

Kamacite always contains more Co than coexisting taenite because Co partitions preferentially into kamacite at all temperatures (Widge and Goldstein 1977). In a zoned taenite + kamacite particle, kamacite Co concentrations increase through the H (0.4–0.5 wt%) → L (0.7–1.0 wt%) → LL (1.5–3 wt%) sequence. This trend can be understood in terms of chondrite bulk metal compositions. Fe becomes oxidized and incorporated into silicates through the H → L → LL sequence. The total amount of metal, therefore, decreases, and the residual metal becomes progressively enriched in Ni and Co through this sequence. The lever rule shows that the kamacite:taenite ratio decreases through the H → L → LL sequence (Fig. 1). Co partitions into a decreasing kamacite fraction through this sequence, causing the kamacite grains to become progressively enriched in Co. For the same reason, zoneless plessite particles in L group chondrites have higher kamacite Co concentrations (0.6–1.0 wt%) than zoneless plessite particles in H group chondrites (0.4–0.6 wt%).

CONCLUSIONS

Type 5 and 6 ordinary chondrites from the H and L groups contain 2 types of Fe-Ni metal particles: 1) zoned taenite + kamacite particles; and 2) zoneless plessite particles, which lack systematic Ni zoning and consist of tetrataenite in

a kamacite matrix. The 2 types of metal particles commonly exist in close proximity within the same ordinary chondrite.

The microstructures of ordinary chondrite metal particles (P-poor) are the result of metamorphic heating and cooling in a parent body. Polycrystalline taenite may have formed by impact induced recrystallization or by sintering of chondrule and matrix metal during metamorphism. Metal particles experienced taenite grain coarsening during metamorphism, commonly becoming monocrystalline taenite particles in type 5 and 6 ordinary chondrites. All taenite particles (monocrystalline or polycrystalline) experienced homogenization within and between particles during metamorphism.

The taenite transformations that occurred during cooling from peak metamorphic temperatures depend on whether parent taenite was polycrystalline or monocrystalline. Polycrystalline taenite particles transformed to zoned taenite + kamacite particles by kamacite nucleation at taenite/taenite grain boundaries during cooling. Monocrystalline taenite particles transformed to zoneless plessite particles by martensite formation and subsequent martensite decomposition to tetrataenite and kamacite during the same cooling process. The presence of zoneless plessite particles in type 5 and 6 ordinary chondrites is entirely consistent with slow cooling after metamorphism and cannot be explained by hot accretion-autometamorphism, post-metamorphic brecciation, or shock processing. The phase transformations responsible for the formation of zoned taenite + kamacite particles and zoneless plessite particles are consistent with experimental studies of Fe-Ni alloys that are compositionally similar to metal in ordinary chondrites (Reisener and Goldstein 2003).

Acknowledgments–This research was supported by NASA grant #NAG5–11778, J. I. Goldstein, principal investigator. The authors appreciate helpful reviews given by A. Kracher, A. Rubin, and especially E. Scott.

Editorial Handling—Dr. Edward Scott

REFERENCES

Aaron H. B. and Aaronson H. I. 1968. Growth of grain boundary precipitates in Al-4% Cu by interfacial diffusion. *Acta Metallurgica* 16:789–798.

Agrell S. O., Long J. V., and Ogilvie R. E. 1963. Nickel content of kamacite near the interface with taenite in iron meteorites. *Nature* 198:749–750.

Bennett M. E. I. and McSween H. Y. 1996. Shock features in iron-nickel metal and troilite of L-group ordinary chondrites. *Meteoritics & Planetary Science* 31:255–264.

Bevan A. 1983. Chemical and mineralogical studies of metal in meteorites. Ph.D. Thesis, University of London, London, England.

Buchwald V. F. 1975. *Handbook of iron meteorites. Their history, distribution, composition, and structure.* Berkeley: University California Press. 1418 p.

Grokhovsky V. J. and Bevan A. W. R. 1983. Plessite formation by discontinuous precipitation reaction from γ-Fe, Ni in Richardton (H5) ordinary chondrite. *Nature* 301:322–324.

Hopfe W. D. and Goldstein J. I. 2001. The metallographic cooling rate method revised: Application to iron meteorites and mesosiderites. *Meteoritics & Planetary Science* 36:135–154.

Hutchison R. and Bevan A. W. R. 1983. Conditions and time of chondrule accretion. In *Chondrules and their origins,* edited by King E. A. Houston: Lunar and Planetary Institute. pp. 1162–1179.

Jarosewich E. 1990. Chemical analyses of meteorites: A compilation of stony and iron meteorite analyses. *Meteoritics* 25:323–337.

Kachi S, Bando Y., and Higuchi S. 1962. The phase transformation of iron-rich iron-nickel alloy in fine particles. *Japanese Journal of Applied Physics* 1:307–313.

Kajiwara S., Ohno S., Homa K., and Uda M. 1987. Martensitic transformation in ultrafine particles of pure Co and Co-Fe alloys. Proceedings, Phase Transformations 87:216–219.

Kajiwara S., Ohno S., and Homa K. 1991. Martensitic transformations in ultrafine particles of metals and alloys. *Philosophical Magazine A* 63:625–644.

Kaufman L. and Cohen M. 1956. The martensitic transformation in the iron-nickel system. *Transactions of the American Institute of Mining and Metallurgical Engineers* 206:1393–1401.

Kring D. A., Hill D. H., Gleason J. D., Britt D. T., Consolmagno G. J., Farmer M., Wilson S., and Haag R. 1999. Portales Valley; A meteoritic sample of the brecciated and metal-veined floor of an impact crater on an H chondrite asteroid. *Meteoritics & Planetary Science* 34:663–669.

Massalski T. B., Park F. R., and Vassamillet L. F. 1966. Speculations about plessite. *Geochimica et Cosmochimica Acta* 30:649–662.

McCoy T. J., Scott E. R. D., Jones R. H., Keil K., and Taylor G. J. 1991. Composition of chondrule silicates in LL3–5 chondrites and implications for the nebular history and parent body metamorphism. *Geochimica et Cosmochimica Acta* 55:601–619.

McSween H. Y., Sears D. W. G, and Dodd R. T. 1988. Thermal metamorphism. In *Meteorites and the early solar system,* edited by Kerridge J. F. and Matthews M. S. Tucson: University of Arizona Press. pp. 102–113.

Rancourt D. G., Lagarec K., Densmore A., Dunlap R. A., Goldstein J. I., Reisener R. J., and Scorzelli R. B. 1999. Experimental proof of the distinct electronic structure of a new meteoritic Fe-Ni alloy phase. *Journal of Magnetism and Magnetic Materials* 191:L255–L260.

Reed S. J. B. 1964. Composition of the metallic phases in some stone and stony-iron meteorites. *Nature* 204:374–375.

Reed-Hill R. E. 1964. *Physical metallurgy principles.* Princeton: D. Van Nostrand Company, Inc. 630 p.

Reisener R. J. and Goldstein J. I. 1999a. Microstructural and chemical study of Fe-Ni metal inside Semarkona chondrules (abstract). 30th Lunar and Planetary Science Conference. pp. 1868–1869.

Reisener R. J. and Goldstein J. I. 1999b. The evolution of metal in chondrites during prograde metamorphism: The role of vapor phase transport (abstract). *Meteoritics & Planetary Science* 34: A97–A98.

Reisener R. J. and Goldstein J. I. 2003. Ordinary chondrite metallography: Part 1. Fe-Ni taenite cooling experiments. *Meteoritics & Planetary Science.* This issue.

Reisener R. J., Petaev M. I., and Goldstein J. I. 2001. Olivine zoning and retrograde olivine-orthopyroxene-metal equilibration in types 5 and 6 ordinary chondrites (abstract #1735). 32nd Lunar and Planetary Science Conference.

Romig A. D. and Goldstein J. I. 1981. The diffusivity of Ni in Fe-Ni and Fe-Ni-P martensites. *Metallurgical and Materials Transactions A* 12:243–251.

Rubin A. E. 1990. Kamacite and olivine in ordinary chondrites: Intergroup and intragroup relationships. *Geochimica et Cosmochimica Acta* 54:1217–1232.

Rubin A. E. 1994. Metallic copper in ordinary chondrites. *Meteoritics* 29:93–98.

Rubin A. E. and Brearley A. J. 1996. A critical evaluation of the evidence for hot accretion. *Icarus* 124:86–96.

Rubin A. E., Ulff-Moller F., Wasson J. T., Carlson W. D. 2001. The Portales Valley Meteorite breccia: Evidence for impact-induced melting and metamorphism of an ordinary chondrite. *Geochimica et Cosmochimica Acta* 65:323–342.

Scott E. R. D. 1982. Origin of rapidly solidified metal-troilite grains in chondrites and iron meteorites. *Geochimica et Cosmochimica Acta* 46:813–823.

Scott E. R. D. and Rajan R. S. 1981. Metallic minerals, thermal histories, and parent bodies of some xenolithic, ordinary chondrites. *Geochimica et Cosmochimica Acta* 45:53–67.

Scott E. R. D., Lusby D., and Keil K. 1985. Ubiquitous brecciation after metamorphism in equilibrated ordinary chondrites. *Journal of Geophysical Research* 90:D137–D148.

Sears D. W. and Axon H. J. 1975. The metal content of common chondrites (abstract). *Meteoritics* 10:486–487.

Shewmon P. G. 1989. Diffusion in solids. Warrendale: The Minerals, Metals & Materials Society. 246 p.

Smith B. A. and Goldstein J. I. 1977. The metallic microstructures and thermal histories of severely reheated chondrites. *Geochimica et Cosmochimica Acta* 41:1061–1072.

Stöffler D., Keil K., and Scott E. R. D. 1991. Shock metamorphism of ordinary chondrites. *Geochimica et Cosmochimica Acta* 55: 3845–3867.

Taylor G. J., Maggiore P. L., Scott E. R. D., Rubin A. E., and Keil K. 1987. Original structures and fragmentation and reassembly histories of asteroids: Evidence from meteorites. *Icarus* 69:1–13.

Turnbull D. 1955. Role of structural impurities in phase transformations. In *Impurities and imperfections*. Columbus: American Society for Metals. pp. 121–144.

Widge S. and Goldstein J. I. 1977. Redetermination of the Fe-rich portion of the Fe-Ni-Co phase diagram. *Metallurgical and Materials Transactions A* 8:309–315.

Willis J. and Goldstein J. I. 1981. A revision of metallographic cooling rate curves for chondrites. Proceedings, 12th Lunar and Planetary Science Conference. pp. 1135–1143.

Willis J. and Goldstein J. I. 1983. A three-dimensional study of metal grains in equilibrated, ordinary chondrite. Proceedings, 14th Lunar and Planetary Science Conference. *Journal of Geophysical Research* 88:287–292.

Wood J. 1967. Chondrites: Their metallic minerals, thermal histories, and parent planets. *Icarus* 6:1–49.

Yang C. W., Williams D. B., and Goldstein J. I. 1997. Low temperature phase decomposition in metal from iron, stony iron, and stony meteorites. *Geochimica et Cosmochimica Acta* 61: 2943–2956.

Zhou Y. H., Harmelin M., and Bigot J. 1990. Martensitic transformation in ultrafine Fe-Ni powders. *Materials Science and Engineering A* 124:241–249.

Zhou Y. H. and Harmelin M., and Bigot J. 1991. Preparation of ultrafine metallic powders. A study of the structural transformations and the sintering behavior. *Materials Science and Engineering A* 133:775–779.